NEUROExos: a powered elbow exoskeleton for physical rehabilitation

Nicola Vitiello, *Member, IEEE*, Tommaso Lenzi, *Student Member, IEEE*, Stefano Roccella, Stefano Marco Maria De Rossi, *Student Member, IEEE*, Emanuele Cattin, Francesco Giovacchini, Fabrizio Vecchi, *Member, IEEE*, Maria Chiara Carrozza, *Member, IEEE*

Abstract — **This paper presents the design and experimental test of the robotic elbow exoskeleton NEUROExos (NEUROBOTICS Elbow Exoskeleton). The design of NEUROExos was focused on three solutions which enable its use for post-stroke physical rehabilitation. Firstly, double-shelled links allow an ergonomic physical human-robot interface, and consequently a comfortable interaction. Secondly, a 4-degree-of-freedom passive mechanism, embedded in the link, allows the user's elbow and robot axes to be constantly aligned during movement. The robot axis can passively rotate on the frontal and horizontal planes 30° and 40° respectively, and translate on the horizontal plane 30 millimeters. Finally, a variable impedance antagonistic actuation system allows NEUROExos to be controlled with two alternative strategies: independent control of the joint position and stiffness, for robot-in-charge rehabilitation mode, and near-zero impedance torque control, for patient-in-charge rehabilitation mode. In robot-in-charge mode, the passive joint stiffness can be changed in the range 24-56 N·m/rad. In patient-in-charge mode, NEUROExos output impedance ranges from 1 N·m/rad, for 0.3 Hz motion, to 10 N·m/rad, for 3.2 Hz motion.**

Index Terms — **Rehabilitation Robotics, Wearable Robotics, Smart Actuators, Human-Robot Joint Axes Self-Alignment, Physical Human-Robot Interaction.**

I. INTRODUCTION

Stroke is the major cause of adult long-term disability in Europe and many other countries [1]-[3] and strains national services and related costs [4]-[6]. In about 85% of cases, stroke causes hemiparesis in subjects, resulting in impairment of the upper limb and disabilities in performing activities of daily living, with consequent medical and social care consuming a huge amount of healthcare resources [7].

Robot-aided physical rehabilitation has been proposed to support the physicians in providing high-intensity therapy, consisting of repetitive movements of the impaired limb [7]-[9]. Robots can allow patients to receive a more effective and stable rehabilitation process, and therapists to reduce their workload. Robots can also offer reliable tools for functional assessment of patient progress and recovery by measuring physical parameters, such as speed, direction, and strength of patient residual voluntary activity [10]. Robot-aided rehabilitation is slowly convincing the community of therapists to be as good as or even better than manual therapy [10]-[12].

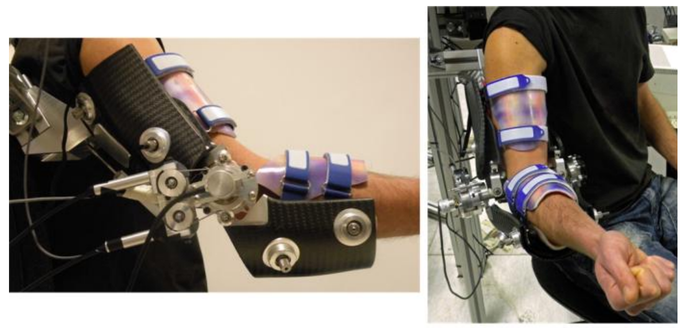

(a) (b)

Fig. 1 Overview of NEUROExos: (a) lateral view, (b) front view.

Common architectures of rehabilitation robots include: end-point manipulators [11], [13]-[16], cable suspensions [17]-[19], and powered exoskeletons [20]-[33]. Among these, powered exoskeletons, despite their higher system complexity, can provide assistance independently to each user's joint. This allows to better retrain the correct physiological muscle-skeletal synergies, minimizing and controlling any compensatory movement.

An exoskeleton for post-stroke physical rehabilitation is a non-portable mechanical device that is anthropomorphic in nature, is "worn" by the user and fits closely to his or her body [33]. Given the close interaction with the user, comfort is a major concern. The robot should be lightweight and take into account the user's joints range of motion (ROM), anthropometry, and kinematics [32], [34]. The physical human-robot interaction (pHRI) area should be large and match the shape of the patient's limb, to reduce the pressure on the user's skin [27], [35]. Furthermore, the actuation and control of the robot should allow safe execution of rehabilitation exercises in two modes of operation: *robot-in-charge*, when the robot is driving the subject in doing the

Manuscript received on April 29, 2012. This work was partly supported by: EU within the NEUROBOTICS Integrated Project (FP6-IST-FET Project #2003-001917), the EVRYON Project (FP7/2007-2013 Grant Agreement num. 231451) and the CYBERLEGs Project (FP7/2007-2013 Grant Agreement num. 287894); and Regione Toscana under the Health Regional Research Programme 2009 within the project EARLYREHAB.

All authors are with The BioRobotics Institute, Scuola Superiore Sant'Anna, viale Rinaldo Piaggio, 34, 56025, Pontedera (PI), Italy. Nicola Vitiello is corresponding author to provide phone: +39 050 883472; fax: +39050 883 497; e-mail: n.vitiello@sssup.it. Emanuele Cattin was with The BioRobotics Institute (formerly ARTS Lab) of Scuola Superiore Sant'Anna, viale Rinaldo Piaggio, 34, 56025, Pontedera (PI), Italy, until 2009.

exercises, and *patient-in-charge*, when the subject is driving the robot that is only partially assisting the movement [11].

In this paper we introduce NEUROExos, a novel elbow powered exoskeleton (see Fig. 1) designed for post-stroke rehabilitation of the arm, ensuring maximum comfort and safety to the patient. NEUROExos presents three innovative design solutions:

1. a compact and light-weight mechanical structure with double-shelled links, with a wide pHRI area to minimize the pressure on the skin;
2. a 4-degree-of-freedom passive mechanism that unloads the elbow articulation from undesired loads by ensuring the alignment of human and robot joint axes;
3. an antagonistic, compliant remote actuation system with an independent joint position and stiffness control (for robot-in-charge exercises) and a near-zero impedance torque control (for patient-in-charge exercises).

In the paper we also present the results of the experimental characterization carried out to assess: the suitability of the pHRI area for a comfortable interaction, the functionality of the 4-DOF passive mechanism by comparing its degree of laxity with the one of the human elbow axis, and the performance of the actuation, sensory and control system.

NEUROExos was previously introduced by two conference papers: in [36] we gave an overview of the design paradigm, and in [37] we presented the passive compliance controller. NEUROExos was also used as a test bed for control algorithms and sensory system: in [38]-[40] we used it to test two different algorithms for detecting user motor intentions, and in [41] to validate a new sensing technology for measuring human-robot interaction pressure onto a wide tailored interaction surface.

The design of NEUROExos is described in Section II, results of the experimental characterization are reported in Section III and are discussed in Section IV. Finally, Section V draws the conclusions.

II. The NEUROExos platform

This section presents the main technical solutions of NEUROExos. Five subsystems are implemented on the platform and described hereafter: the double-shelled link structure, the 4-DOF passive mechanism, the antagonistic tendon-driven compliant actuation, and the control and sensory systems.

A. Double-shelled links

Most upper-limb powered exoskeletons are made of bar-shaped links, coupled with the user's limb segments through multiple orthotic shells or cuffs [26]-[32]. This solution, while simple, introduces problems in terms of encumbrance, inertia, and kinematic compatibility with the limb, resulting in a poor wearability of the robot. To overcome these limitations, the links of NEUROExos are made of a double-shelled structure (Fig. 2-a) composed of two concentric shells (inner and outer shells).

Outer shells provide structural stiffness and strength to the robot, and transfer the load to the human limb segments.

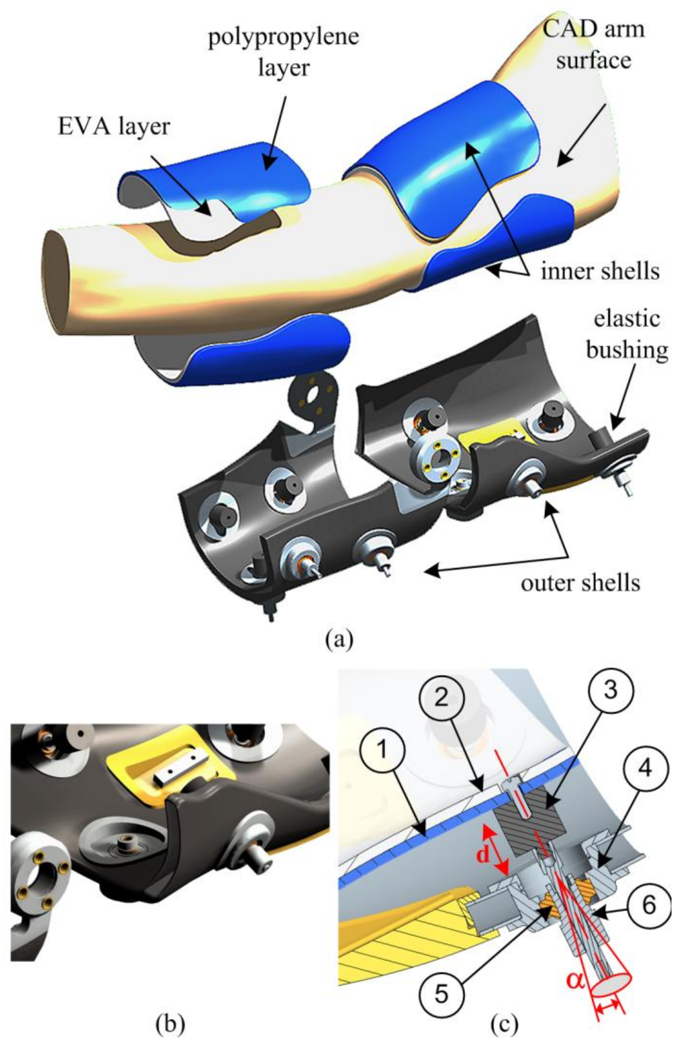

Fig. 2 Double-shelled links: (a) exploded view of the links, (b) zoom on the double-walled carbon-fiber structure of outer shells, and (c) section view of the mechanism connecting outer and inner shells: (1) layer of polypropylene, (2) layer of ethylene vinyl acetate (EVA), (3) elastic bushing, (4) aluminium frame, (5) spherical joint, (6) threaded rod.

Compared with bar links, shell-shaped links have their center of mass closer to the longitudinal axis of the human limb segment thanks to an optimized material distribution around the limb segment. This reduces the possibility that the assistive load applies an uncomfortable torque about the longitudinal axis of the human limb segment.

Inner shells are in direct contact with the user's arm to transfer the loads. Thanks to the use of a soft orthopaedic material and a wide interaction area, they contribute to reduce the pressure on the user's skin and ensure a comfortable interaction [41].

1) Inner shells

Each inner shell is made of two half-shells, coupled with the dorsal and ventral sides of the arm (Fig. 2-a) and fastened with velcro belts, as shown in Fig. 1. Inner shells have a two-layered structure: a 3 mm-thick internal layer of ethylene vinyl acetate (555XEB/3, M.T.O., Italy), for moisture draining and skin transpiration, and a 3 mm-thick outer layer of polypropylene (558/3 M.T.O., Italy). Inner shells come in different sizes, and can also be tailor-made on each subject (e.g. by thermo-shaping a polypropylene layer).

2) Outer shells

Outer shells have a double-walled carbon fibre structure, which has total height of 10 millimeters and thickness of 1.5 millimeters (see Fig. 2-b). Size and shape of the NEUROExos outer shells were designed by using a 3D model of the human arm surface. This surface was obtained by laser-scanning (INKAY, Italy) and digitalization (Pro/Engineer, PTC, MA, USA) of the arm surface of a voluteer (male, height 175 cm, weight 75 kg). Outer shells can be connected to inner shells of different shapes, and, therefore, allow the same exoskeleton links to be used by several users. Outer shells also house the aluminium frames of the 4-DOF passive mechanism, the gear box for the active flexion-extension DOF, and the inner-outer shell connecting elements (Fig. 2-a).

NEUROExos upper-arm and forearm links (including all actuation and mechanics components) have a total weight of 1.65 kg and 0.65 kg respectively, and the moment of inertia of the forearm link about the flexion-extension axis is equal to $7.2 \cdot 10^{-3}$ kg·m^2.

3) Inner-outer shell connecting elements

The connection between inner and outer shells is obtained through a small mechanism that allows small relative adjustments.

The connection is depicted in Fig. 2-c. An aluminium frame is embedded within the carbon fiber structure and houses a ball joint (GE 8C, SKF, Sweden). A threaded rod passes through the ball joint and is screwed into an elastic bushing (Radialflex M4, Paulstra, France), which is connected to the inner shell. Turning the threaded rod allows the regulation of the inter-shell distance (dimension d in Fig. 2-c) in a range of 15 millimiters. Four connecting mechanisms are used for each couple of inner-outer shells. The relative spatial orientation between inner and outer shells is set by independently changing the distance d at each connection point. Passive ball joints allow the rods to passively tilt of a maximum angle α of 15° (see Fig. 2-c), thus preventing the inner shells from being strained. Elastic bushings provide the connecting mechanisms with a high longitudinal (along the threaded rod longitudinal axis) compression stiffness (100 N/mm), which is needed for load transferring between inner and outer shells, and a low tangential stiffness (15 N/mm) allowing small relative sliding motions between shells.

B. The 4-DOF passive mechanism

Exoskeletal machines are worn by the user, therefore they should match the constraints given by the kinematics of the limb to be assisted because misalignements between human and robot joint rotation axes can cause translational forces at the pHRI surface [43]. These translational forces are highly undesired, since they load the skin and the muscleskeletal system, and make the interaction uncomfortable or even painful [34].

The problem of joint axes misalignment is particularly critical in exoskeletons interacting with the upper limb in multiple points (i.e. hand, forearm, upper-arm, and/or trunk).

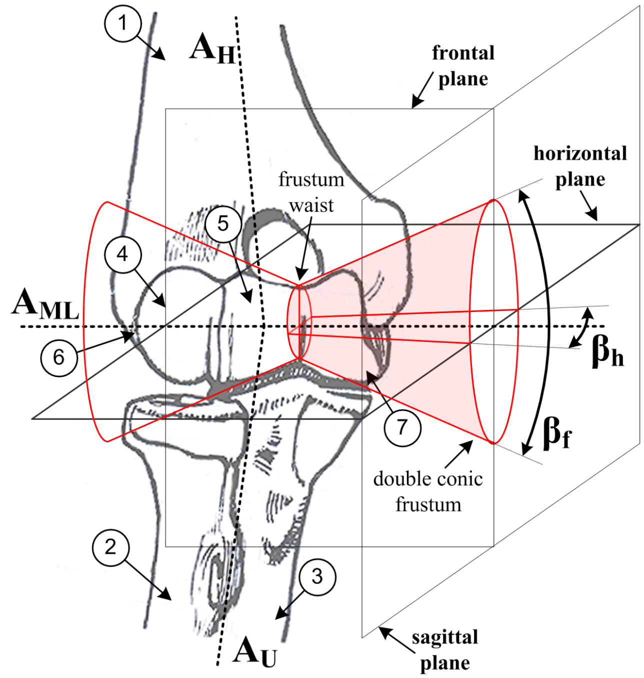

Fig. 3 Anatomy of the human elbow: (1) humerus, (2) radius, (3) ulna, (4) capitellum, (5) throclea, (6) lateral facet of capitellum, (7) lateral facet of trochlea. A_H is the humerus longitudinal axis, A_U is the ulna longitudinal axis, A_{ML} is the anatomical medial-lateral axis passing from the capitellum center to the trochlear center [46], β_h and β_f are the frustum vertex angles respectively on the horizontal and frontal planes (adapted from [71]).

Given that each limb segment is connected rigidly to the robot, translational forces are entirely unloaded on the user's skin and articulation. A correct alignment is difficult to achieve in exoskeletons, given that the exact location and orientation of human joint axes cannot be detected from the outside without complex imaging techniques. Moreover, many human joints do not behave as simple hinges, changing the spatial configuration of their rotation axis along with the joint motion.

The misalignment problem has been often addressed by designing specific kinematics schemes [26], [28]-[31] or joints [27], [32]. However, a more general methodology to address this issue has been proposed in [34]. The basic idea consists of mounting the active rotational joint on a moveable translational passive mechanism which decouples the robot joint rotations from axis translations. Translational passive mechanisms unload human limb segments and articulations from undesired translational forces, while the rotational active joints transfer the assistive torques onto the human joints [34].

This solution, however, does not take into account the laxity of the elbow articulation. Elbow laxity has been widely investigated in orthopedics studies, showing that elbow articulation behaves as a "loose hinge joint" [44]-[46]. Over the flexion-extention motion range, the elbow rotation axis is not firm, but traces the surface of a double quasi-conic frustum with an elliptical cross-section [44]-[45] (see Fig. 3). The double frustum has both an inter- and intra-individual variability, the latter being determined by: the flexion mode (active or passive motion of the joint), the forearm position (pronated or supinated) and any varus or valgus torque loading

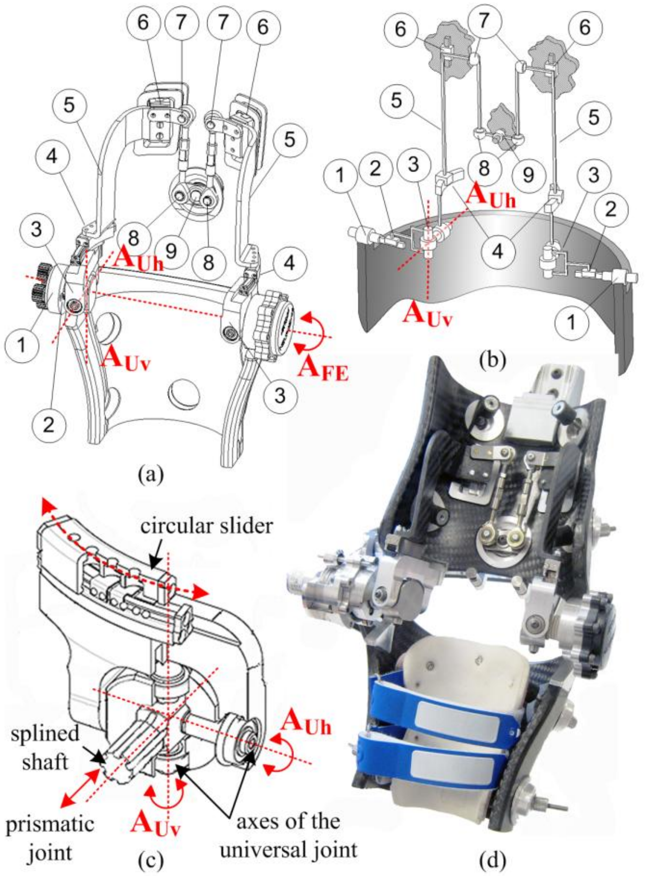

Fig. 4 Schematic drawings and pictures describing the strucutre and working principles of the NEUROExos 4-DOF passive mechanism: (a) CAD and (b) layout of the passive mechanism: (1) NEUROExos flexion-extension joint, axis A_{FE}, (2) prismatic joint trough splined shaft, (3) universal joint, (4) circular slider, (5) carbon fiber link, (6) linear slider, (7) spherical joint, (8) spherical joint, (9) rotational joint, (c) zoom on joins (1), (2), (3) and (4): A_{Uv} and A_{Uh} are the vertical and horizontal rotational axes of the universal joint, the splined shaft allows for the prismatic joint (2) whose axis coincides with A_{FE}, (d) implementation of the passive mechanism.

the articulation. In particular, the frustum vertex angles β_f, on the frontal plane, and β_h, on the horizontal plane, assume a maximum value of about 10° and 6° respectively. In addition, the elbow average rotation axis over a full flexion-extension task forms an angle of 80°-92° with the humerus longitudinal axis A_H onto the frontal plane, and an angle of ±5° with the medial-lateral anatomic axis A_{ML} onto the horizontal plane.

Starting from the variability of the human elbow laxity, we designed a 4-DOF passive mechanism which provides the NEUROExos powered axis with the same degree of laxity of the human elbow. Thanks to this passive mechanism, the active axis can trace a double conoid whose frustum vertex angles satisfy both the intra- and inter-subject variability of elbow axis laxity. In addition, two passive translational DOFs unload the elbow articulation from undesired translational forces.

The passive mechanism scheme along with its implementation is depicted in Fig. 4. The mechanism consists of a closed-chain composed of 13 passive joints: 4 prismatic, 4 spherical, 2 circular sliders, 2 universal and 1 rotational joint.

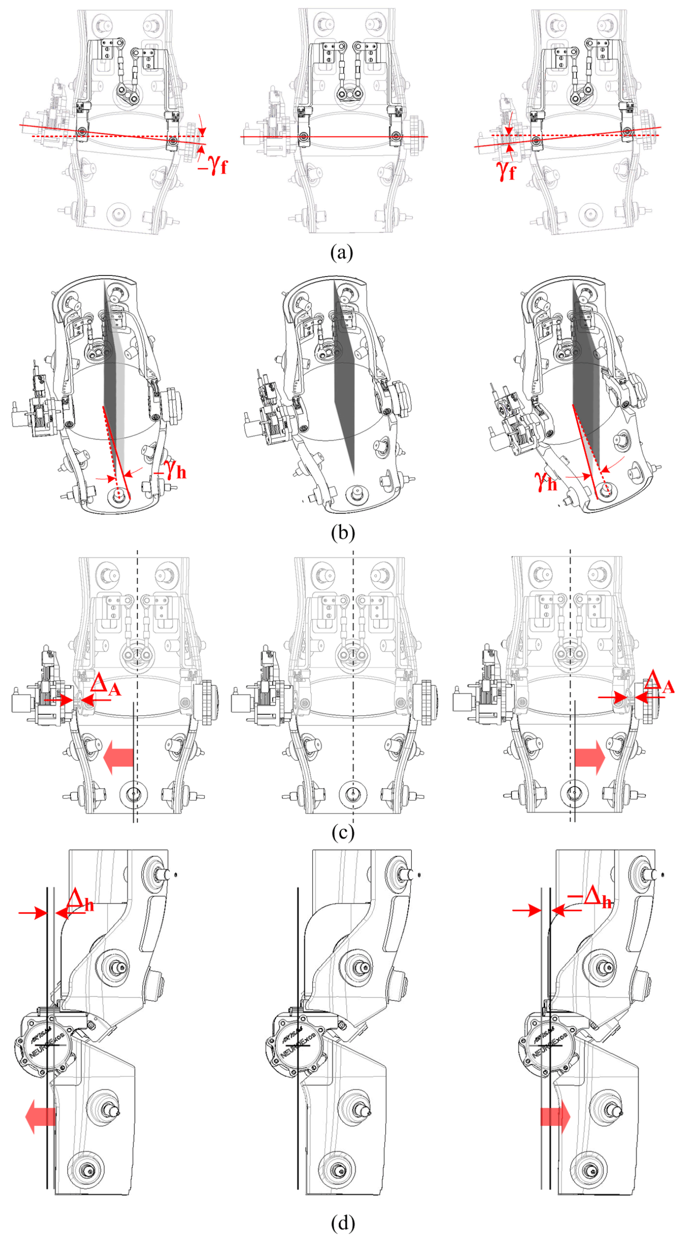

Fig. 5 Description of the passive movements obtained by means of the NEUROExos 4-DOF passive mechanism: (a) rotation in the frontal plane, (b) rotation in the horizontal plane, (c) translation of the forearm link along the flexion-extension axis, and (d) translation in the horizontal plane.

Despite its complexity, this compact mechanism fits within the space between upper-arm inner and outer shells, and therefore does not affect the overall system encumbrance.

NEUROExos flexion-extension axis A_{FE} is identified by the two axes of the prismatic joints labeled as 2 in Fig. 4. These joints are implemented by means of two splined shaft-hole couplings having a ROM of 35 millimeters. Each splined shaft is attached to a universal joint (labeled as 3, see Fig. 4), whose ROM is 100° around its horizontal axis (A_{Uh}) and 24° around its vertical axis (A_{Uv}) (see Fig. 4-c). Each fork housing a universal joint is then attached to a slider (joint number 4 in Fig. 4) which moves along a circular trajectory having a diameter of 120 millimeters and an angular ROM of 42°.

Through an L-shaped carbon fiber link, the circular slider is connected to a linear slider (joint number 6, ROM of 30 millimeters). The linear slider is linked to the rotational joint labeled as 9 (ROM of 40°) by means of two spherical joints (male threaded, maintenance-free rod ends, SKF, Göteborg, Sweden), labeled as 7 and 8, connected by a bar with an adjustable length.

The passive mechanism provides four DOFs as depicted in Fig. 5. Three DOFs are used to allow the NEUROExos axis A_{FE} to trace a double conic frustum:

1. A_{FE} can rotate in the frontal plane of an angle $\gamma_f = \pm 15°$ (see Fig. 5-a);
2. A_{FE} can rotate in the horizontal plane of an angle $\gamma_h = \pm 21°$ (see Fig. 5-b);
3. the NEUROExos forearm link can slide along the axis A_{FE} of a distance of ±15 mm (see Fig. 5-c).

This latter DOF, which is determined by the prismatic joints labeled as 2 in Fig. 4, allows the self-alignment of the waist of the double quasi-conic frustum traced by the elbow axis with the vertex of the double conoid traced by the NEUROExos axis along the anatomical medial-lateral axis A_{ML}.

The fourth DOF, shown in Fig. 5-d, allows the A_{FE} to translate on the horizontal plane along the antero-posterior direction of a segment $\Delta_h = \pm 15$ mm. Therefore it allows any undesired translational force acting on this direction to be unloaded [34].

Finally, the elastic bushings of NEUROExos allow the user's upper arm (rigidly connected to the upper inner shell) to slide against the NEUROExos upper shell. This way an additional DOF is given to the NEUROExos axis A_{FE} which unloads the subject's articulation from the frontal-plane component of the undesired translational force.

C. Antagonistic compliant actuation

The actuation and control system of an exoskeleton for post-stroke physical rehabilitation should provide two different therapy protocols. The two modalities can be described as *robot-in-charge* and *patient-in-charge* [47], [48]. In robot-in-charge mode, which is usually implemented in the initial stage of the rehabilitation process when patients cannot move autonomously, the robot should be able to promote a desired motion pattern. This modality requires the robot to have relatively high joint impedance. Patient-in-charge mode is needed when the subject can control some movements of his/her limb, and requires some assistance from the system to complete the task. In this latter case, the robot should not hinder the patient motion, but rather it should show near-zero impedance while assisting the user. Therefore it is fundamental to provide the robot with impedance control.

Active control of impedance can be achieved using rigid actuation systems, such as geared electric motors, and a closed-loop torque control. Unfortunately, beyond the closed-loop control bandwidth, the system will show high inherent impedance [27]-[28], which raises strong safety issues [49]. Series elastic actuators have been successfully applied in this field to solve safety issues [47], [48], [50], [51]. In this case, the actuation is not rigid and allows relatively low joint impedance across the entire frequency spectrum. However, variations in the output impedance can still be achieved only by means of closed-loop interaction control strategies [49].

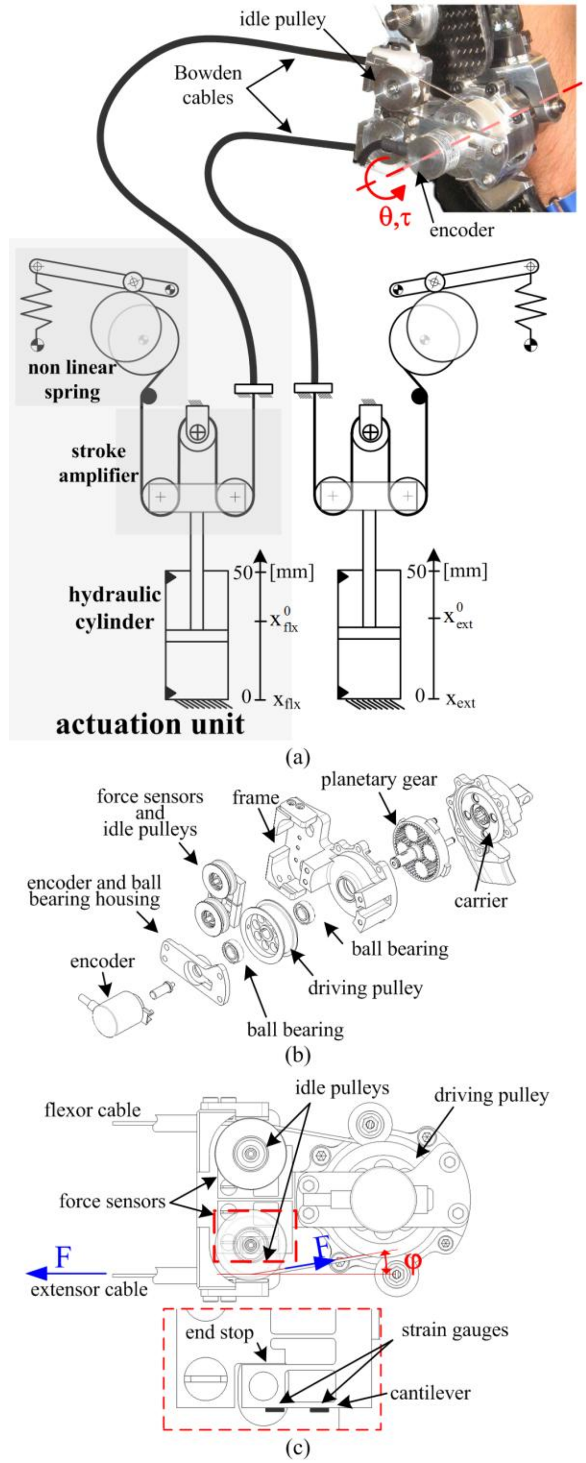

Fig. 6 Schematic drawing of the antagonistic tendon-driven compliant actuation and sensory system of the NEUROExos: (a) two remote antagonistic units, named flexor ('flx') and extensor ('ext'), power the NEUROExos active joint, (b) exploded view of the driving block, and (c) working principle of the cable force sensors.

The so called "actively-adjustable passive compliance" actuators [52]-[55] overcome these limitations. This kind of actuation system can provide software-controllable hardware compliance, simplifying the control system, minimizing the risk of instabilities of active impedance control, and guaranteeing maximum safety in the interaction with the robot. The adjustable compliant behavior of this actuator system is obtained by means of an inherent hardware property of the actuation, requiring no closed-loop control.

NEUROExos is powered by an antagonistic-driven compliant joint (ADCJ), an actively-adjustable passive compliance actuator successfully exploited in [20], [25]. The ADCJ is powered by two antagonist actuation units, each showing a non-linear elastic behaviour with an adjustable resting position.

The layout of the ADCJ implemented on NEUROExos is depicted in Fig. 6-a. It consists of a pair of remote and independent antagonistic units [56]-[60]. Each unit consists of a series of: a non-linear elastic mechanism with a quadratic force (F) vs. cable elongation (Δl) function ($F(\Delta l) = b_1 \Delta l^2 + b_2 \Delta l$, with $b_1 = 0.0865$ N/mm^2 and $b_2 = 1.92$ N/mm), a linear hydraulic actuator with a stroke of 50 millimeters (Parker-Hannifin Corp., OH, USA), a stroke amplifier (transforming a hydraulic piston displacement Δx into an elongation of the transmission $\Delta l = a_s \Delta x$, where $a_s = 4$ is the amplification ratio), and a steel-wire rope with a diameter of 1.4 millimeters (Carl Stahl, Süssen, Germany) which transmits the force to the NEUROExos driving block through a Bowden cable.

The non-linear elastic mechanism is based on a linear tension spring coupled with a cam mechanism (see Fig. 6-a), which was presented and characterized in [57]. By using a tension spring of 80 N/mm (T series, D.I.M. srl, Italy) NEUROExos achieves a passive joint stiffness in the range 20-60 N·m/rad. This range is comparable to the one of the human elbow measured in single- [61] and multi-joint arm movements [62] and thus prevents the subject from an uncomfortable (or even painful) interaction with an excessively stiff device in case of involuntary spastic movements. Moreover, the stiffness range of NEUROExos is also comparable to that generated by state-of-the-art end-point manipulators on the elbow [11].

Each hydraulic cylinder is controlled by a three-land-four-way proportional electronic valve, commanded by a ±10 V DC signal, which sets the piston velocity [56], [60]. The hydraulic circuit is powered by a three-phase 1.1 kW AC motor (Parker-Hannifin Corp., OH, USA).

Fig. 6-b shows an exploded view of the driving block, which has a maximum output torque of 15 Nm. This unit is composed by the driving pulley (radius of 19 millimeters), which the antagonistic steel ropes wrap around, a custom-made planetary gear that amplifies the torque by a factor of four, the frame housing the force sensors, and two mechanical end stops that prevent elbow hyperextension and hyperflexion.

Although the planetary gear slightly increases the encumbrance and the inertia of the driving block, its use enables the force transmitted by each antagonist cable to be lowered by a factor of four. This is beneficial for two reasons. First, the lower the trasmitted force, the lower is the friction loss given by the Bowden cables, as outlined in [63] and discussed in our previous works [56]-[60], [64]. In fact, high values of friction would affect the static passive behaviour of the NEUROExos joint when controlled in passive-compliance control mode (see Section E.1): higher the friction, higher the discrepancy between the desired and actual torque field. Second, lowering the transmitted force on the tendon cable also reduces - by the same factor four - the full-scale range of the cable force sensor, which can therefore have smaller size and, consequenlty, the overall design of the driving block can be more compact.

D. Sensory apparatus

A 1024 ppr incremental optical encoder (2420, Kübler, Germany) was assembled coaxially with the driving pulley (see Fig. 6-a and Fig. 6-b) and the sun gear to measure the flexion-extension rotation angle (resolution of 0.022°).

Two custom-made load cells were included in the design to measure the force transmitted by the antagonist tendon cables. In Fig. 6-c the working principle and the layout of the force sensors is depicted. Each antagonist cable comes out from the Bowden cable, passes through an idle pulley, and then wraps on the driving one. The idle pulley is hinged on a shaft rigidly connected to the cantilever of the force sensor and deflects the cable of an angle φ of 15°. Consequently, a component of the cable force F ($2F \cdot \sin(\varphi)$) bends the cantilever. The strain of the cantilever, which is linearly dependant on F, is measured by means of four piezoresistive strain gauges (ESU-025-1000, Entran, England, UK) mounted in full-bridge configuration, and conditioned by a commercial electronics (MecoStrain, MECO, Italy). The mechanical structure of the force sensor was designed to work in safe condition against any overload. In fact, a mechanical end stop prevents the cantilever from becoming loaded over the yield stress and limits the maximum sensed cable force to 200 N. Voltage-to-force curves of the force sensors were characterized and exhibited high linearity (RMSE=0.05 N and R^2=1) and low hysteresis (0.05% of the full-scale range). Peak-to-peak noise was quantified as 0.05 N, constant over the full-scale range.

Two linear potentiometers (SLS095, Penny&Giles, Dorset, UK) are used for the measurement of the piston positions with an accuracy of 0.01 millimeters.

E. Control system

The actuation system of NEUROExos allows for the use of two alternative control strategies: the *passive-compliance control* and the *torque control*, respectively for the execution of robot-in-charge and patient-in-charge exercises.

1) Passive-compliance control

NEUROExos antagonistic actuation and passive-compliance control take inspiration from the human musculoskeletal system, which powers the limbs by using antagonistic muscle pairs. The musculoskeletal system generates a convergent force field around an equilibrium position of the limb by relying on the elastic properties of antagonistic muscles. The selective activation of one of the two muscles displaces the convergent field towards a new equilibrium position and, consequently, changes the position of the limb. The simultaneous co-activation of both muscles (i.e. muscles co-contraction) increases the slope of the convergent field (i.e. the joint stiffness), leaving the limb position unchanged [65]-[69]. In a similar way, the actuation system of NEUROExos can apply a convergent torque field around a certain angular position (i.e. the equilibrium point) by regulating the rest lengths of two opposite elastic actuation lines. The slope of this convergent torque field (i.e. the joint stiffness) can be regulated independently of the equilibrium position, thanks to the non-linearity of the compliant elements [69].

The torque τ applied by the antagonistic cables on the NEUROExos active joint is:

$$\tau = a_{pg} r_{dp} (F_{flx} - F_{ext}) \tag{1}$$

where r_{dp} is the radius of the driving pulley, a_{pg} is the transmission ratio of the planetary gear, and F_{flx} and F_{ext} are the force applied by the flexor and extensor units respectively. Assuming the steel cable is infinitely stiff, the total elongation Δl of the transmission line coincides with the elongation of the non-linear elastic element and, consequently, the force driven by each cable is a non-linear function of the spring elongation:

$$\begin{aligned} F_{ext}(\Delta l_{ext}) &= b_1 \Delta l_{ext}^2 + b_2 \Delta l_{ext} \\ F_{flx}(\Delta l_{flx}) &= b_1 \Delta l_{flx}^2 + b_2 \Delta l_{flx} \end{aligned}. \tag{2}$$

The elongation Δl, of each actuation unit, depends linearly on both the piston position x and the joint angle θ:

$$\begin{aligned} \Delta l_{ext} &= a_s (x_{ext}^0 - x_{ext}) + r_{dp} a_{pg} (\theta - \theta_0) \\ \Delta l_{flx} &= a_s \left(x_{flx}^0 - x_{flx}\right) - r_{dp} a_{pg} (\theta - \theta_0) \end{aligned} \tag{3}$$

where x_{ext} and x_{flx} are the piston positions of the extensor and flexor units respectively, θ_0 is a fixed reference angle, and x_{ext}^0 and x_{flx}^0 are the positions for which the elongations Δl_{ext} and Δl_{flx} are nil when $\theta = \theta_0$ ($\theta \in [0°, 130°]$, and $\theta = \theta_0 = 0°$ corresponds to the configuration of maximum extension).

The joint equilibrium position θ_{eq} is easily calculated by making $\tau = 0$, and substituting (3) in (2):

$$x = a_s \left(\Delta x_{flx} - \Delta x_{ext}\right) / 2 a_{pg} r_{dp} \tag{4}$$

where $\Delta x_{flx} = x_{flx}^0 - x_{flx}$ and $\Delta x_{ext} = x_{ext}^0 - x_{ext}$. By appropriately changing the reference frames for the piston positions, it is possible to have $x_{flx}^0 = x_{ext}^0 = 0$, so that (4) becomes:

$$\theta_{eq} = a_s (x_{ext} - x_{flx}) / 2 a_{pg} r_{dp}. \tag{5}$$

The joint stiffness, defined as $K_\theta = -\partial\tau/\partial\theta$, is equal to:

$$K_\theta = 2 a_{pg}^2 r_{dp}^2 \left(b_2 - b_1 a_s \left(x_{ext} + x_{flx}\right)\right). \tag{6}$$

As equations (5) and (6) show, the joint equilibrium position is proportional to $(x_{ext} - x_{flx})$ while the joint stiffness changes linearly with $(x_{ext} + x_{flx})$. Thereby, the joint equilibrium position and stiffness can be regulated independently.

NEUROExos joint passive compliance is controlled by means of a two-layer hierarchical control system.

The high-level layer is dedicated to the coordination of the piston positions. Given the desired passive compliance, i.e. desired joint equilibrium position (θ_{eq}^{des}) and stiffness (K_θ^{des}), the high-level layer calculates the desired piston positions of both the flexor and extensor units by using two new control variables, which are a linear combination of x_{ext} and x_{flx} (see Fig. 7-a). The *differential-mode command*, is defined as a reciprocal shift of the antagonist pistons:

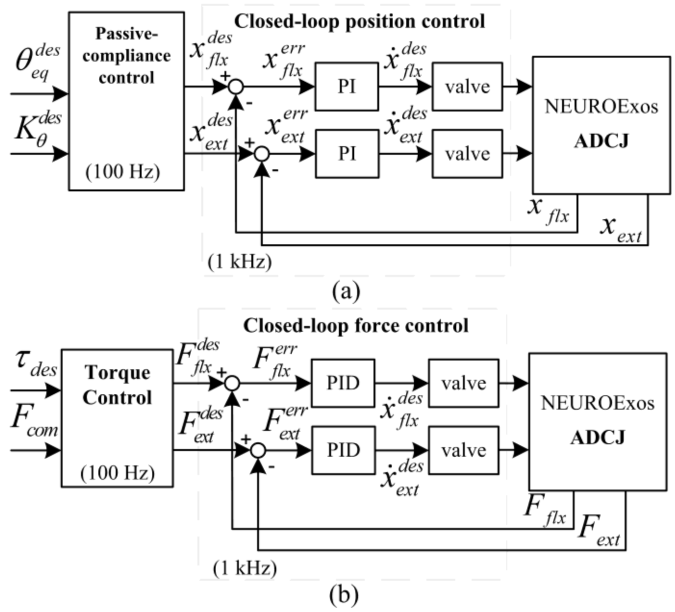

Fig. 7 Block diagram of NEUROExos control strategies: (a) passive-compliance control, (b) torque control.

$$x_{dif} = (x_{ext} - x_{flx}) / 2. \tag{7}$$

The *common-mode command*, is an equal shift of the antagonist pistons:

$$x_{com} = -(x_{ext} + x_{flx}) / 2. \tag{8}$$

Substituting (7) and (8) into (5) and (6), we get the final equations describing how differential- and common-mode commands can be used to respectively control the joint position (9) and stiffness (10):

$$x_{dif} = (a_{pg} r_{dp} / a_s) \theta_{eq} \tag{9}$$

$$x_{com} = \left(K_\theta - 2 a_{pg}^2 r_{dp}^2 b_2\right) / 4 a_{pg}^2 r_{dp}^2 a_s b_1. \tag{10}$$

The differential- and common-mode commands are then converted into piston positions:

$$\begin{aligned} x_{ext}^{des} &= x_{dif} - x_{com} \\ x_{flx}^{des} &= -x_{dif} - x_{com} \end{aligned}. \tag{11}$$

The low-level layer controls the hydraulic piston positions x_{ext} and x_{flx} by means of two independent PI closed-loop regulators [57] with a 20 Hz bandwidth.

In a robot-in-charge task, the passive-compliance controller moves the human elbow by displacing the equilibrium position θ_{eq} of NEUROExos along a desired trajectory. The passive-compliance controller acts in open-loop fashion with respect to θ, and generates a torque field proportional to the $\Delta\theta = \theta_{eq} - \theta$ and K_θ. This way, NEUROExos does not force the position of the human joint (like a position servo would do), but rather it allows deviations from the predefined path: the actual position θ is regulated by the following dynamics equation:

$$I\ddot{\theta} = \tau_{exos} + \tau_h - F_v(\dot{\theta}) - mgL \cdot \sin(\theta + \theta_{off}) \tag{12}$$

where I [N·m·s^2/rad], m [kg] and L [m] denote the inertia, mass and equivalent length of human forearm and hand coupled with the NEUROExos forearm module, g [m/s^2] denotes the constant of gravity, τ_{exos} and τ_h denote respectively the torque applied by the NEUROExos actuation, i.e. $\tau_{exos} = \tau = K_\theta\left(\theta_{eq} - \theta\right)$, and the torque applied by human muscles activation on the elbow, $F_v(\dot{\theta})$ takes into account the friction loss in the planetary gear and the Bowden cables, and θ_{off} is the angle between the longitudinal axis of the upper-arm link and the gravity vector (adjustable in the range [0°,45°] by an external frame).

In quasi-stationary (i.e. $\ddot{\theta} \cong \dot{\theta} \cong 0$) condition and ignoring static friction losses, the actual position θ depends solely on the human muscles activation and the gravity:

$$\tau_{exos} = K_\theta \Delta\theta = mgL \cdot \sin(\theta + \theta_{off}) - \tau_h. \tag{13}$$

In this case, it follows that $\theta = \theta_{eq}$ when $\tau_h = mgL \cdot \sin(\theta + \theta_{off})$, which happens when the human voluntary action balances the gravity action.

2) Torque control

In order to be used for patient-in-charge control strategies, torque control should be able to provide the patient with an assisitve torque with near-zero output impedance, i.e. with minimum to null joint parasitic stiffness.

As shown in the block diagram of Fig. 7-b, the torque control of NEUROExos relies on the independent closed-loop control of the cable force powered by each actuation unit. The desired torque τ_{des} is converted to desired forces on the antagonistic cables by means of the following equation:

$$\begin{aligned} &\text{if } \tau_{des} \geq 0 \Rightarrow \begin{cases} F_{ext}^{des} = F_{com} \\ F_{flx}^{des} = F_{com} + |\Delta F^{des}| \end{cases} \\ &\text{if } \tau_{des} < 0 \Rightarrow \begin{cases} F_{ext}^{des} = F_{com} + |\Delta F^{des}| \\ F_{flx}^{des} = F_{com} \end{cases} \end{aligned} \tag{14}$$

where $F_{com} = \min(F_{flx}, F_{ext})$ is a preload force constantly applied to both the antagonist cables and $\Delta F^{des} = F_{flx}^{des} - F_{ext}^{des} = \tau_{des}/a_{pg}r_{dp}$. Then, the desired cable forces serve as input of two independent closed-loop force controllers. The closed-loop control architecture is that of a classical PID regulator, with a saturation interval of [-0.14, 0.14] m/s for the speed of the hydraulic piston, and an anti-wind-up scheme. The PID regulator operates on the error between the desired and measured cable forces and outputs the speed of the hydraulic piston, which is controlled by means of the DC proportional electro valve (see Section III.C). PID regulators were tuned manually for achieving the widest possible closed-loop bandwidth.

By setting the preload force F_{com} we tune the physical joint stiffness, which is then lowered by the action of the closed-loop controllers. The relationship between preload force and physical stiffness can be obtained by reversing (2)-(3) and applying (6):

$$K_\theta(F_{com}) = 2a_{pg}^2 r_{dp}^2 \left(\sqrt{b_2^2 + 4b_1 F_{com}}\right). \tag{15}$$

3) Control unit and safety loop

NEUROExos controllers run on a real-time control system (PXI-8196 RT, National Instrument, Austin, TX, USA) equipped with a data acquisition card (M-series, National Instrument, Austin, TX, USA). The high-level layers run at 100 Hz, while the low-level closed-loop (position and force) controllers run at 1 kHz. Signals of both cable force and piston positions sensors are sampled at 250 kHz, then low-pass filtered and down-sampled to 1 kHz.

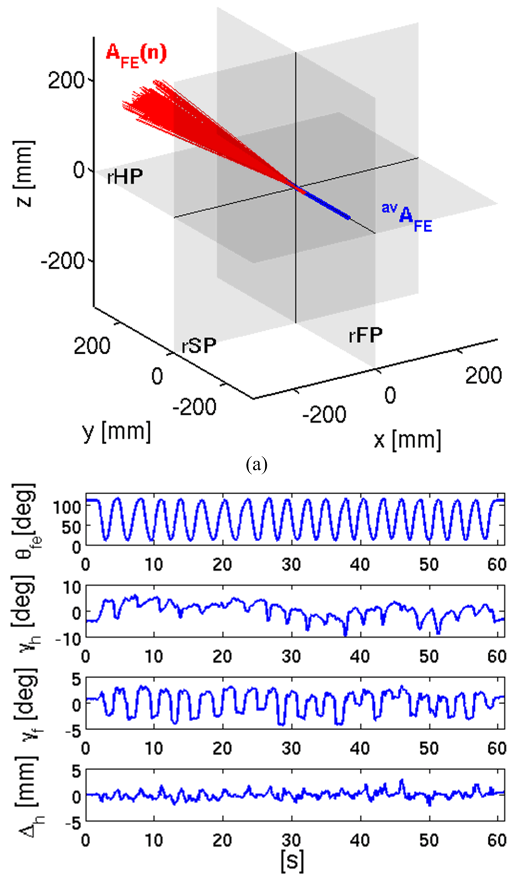

(b)

Fig. 8 Plots of experimental data recorded during the characterization of 4-DOF passive mechanism: (a) reference coordinate system and instantaneous rotation axes $A_{FE}(n)$ for Subject 1, (b) $\theta(t)$, $\Delta_h(t)$, $\gamma_h(t)$ and $\gamma_f(t)$ for Subject 1.

The NEUROExos control system implements a safety loop that switches off the actuation when the force on a cable exceeds 150 N, the joint torque 10 Nm, or the joint speed is greater than 400 deg/s. In addition, in order to detect possible failures of the force sensors and prevent the user from injuries and the system from damages, the safety loop compares the output of the force sensor with an estimate of F obtained through (2) and (3), and switches off the actuation when the difference is more than 30 N.

III. Experimental Characterization

In this section, we characterized the 4-DOF passive mechanism (Section II.B), by testing its effectiveness in aligning the robot with the user's elbow axis, and the performance of the two control strategies (Section II.E).

A. *Characterization of the 4-DOF passive mechanism*

Five healthy subjects (3 males and 2 females) volunteered to participate in the experiment. Each subject wore NEUROExos and performed a cyclical flexion-extension movement (amplitude of about 100°, frequency of about 0.35 Hz, total duration of 120 s). Actuation was unplugged during the experiment. The A_{FE} rotation axis was tracked by means of an optical motion capture system (460, VICON, Oxford, UK) using six passive optical markers. Two markers were placed on upper- and forearm external shells to identify the longitudinal axis of each link. Two markers were applied coaxially to the driving pulley to identify the A_{FE} axis.

The motion of the A_{FE} rotation axis was described in terms of the two angles γ_f and γ_h, which indicate respectively the rotation on the frontal and on the horizontal planes, and a translation Δ_h on the horizontal plane. For each subject and each trial, we applied the following four-step algorithm to identify the horizontal and frontal planes of the human elbow articulation and to compute γ_f, γ_h and Δ_h.

Step 1) For each time sample n between 1 and N, we extracted a geometrical representation of the rotation axis $A_{FE}(n)$, and of the longitudinal segment of the NEUROExos upper-arm $U_A(n)$ and forearm $F_A(n)$ links ($U_A(n)$ is fixed).

Step 2) We calculated the average rotation axis ${}^{av}A_{FE}$ over the entire set of recorded rotation axes $A_{FE}(1 \dots N)$.

Step 3) We identified three orthogonal datum planes. Among the infinite planes orthogonal to ${}^{av}A_{FE}$, the *reference Sagittal Plane* (rSP) was chosen to minimize the average distance between the intersection points of $A_{FE}(1 \dots N)$ and rSP with ${}^{av}A_{FE}$. The *reference Frontal Plane* (rFP) was defined as the plane orthogonal to rSP which passes trough ${}^{av}A_{FE}$ and the segment U_A. Finally, a *reference Horizontal Plane* (rHP) was defined to be orthogonal to both rSP and rFP, and passing through ${}^{av}A_{FE}$. In Fig. 8-a, the three datum planes along with $A_{FE}(1 \dots N)$ are depicted for Subject 1.

Step 4) We computed $\gamma_f(n)$ as the angle between rFP and the projection of $A_{FE}(n)$ on rSP. Likewise, $\gamma_h(n)$ was calculated as the angle between rHP and the projection of $A_{FE}(n)$ on rSP. $\Delta_h(n)$ is obtained from the projection of the distance between $A_{FE}(n)$ and ${}^{av}A_{FE}$ onto rHP.

Fig. 8-b shows the position of A_{FE} for Subject 1, in terms of γ_h, γ_f and Δ_h, along with the elbow flexion-extension angle θ. Table I reports the mean absolute value, the minimum and maximum of γ_h, γ_f and Δ_h for all subjects, plus the average of these values over all subjects.

B. Characterization of the passive-compliance control

In this Section we evaluate the static and dynamic performances of the passive-compliance control. All the experiments were performed with $\theta_{off} \cong 20°$.

1) Static characterization

The static characterization aims to verify the NEUROExos passive joint stiffness performances in static conditions (i.e. $\dot{\theta} = 0$). The equilibrium position was set to $\theta_{eq} = 45°$, then, for five different common-mode commands (i.e. $x_{com} \in \{0,1,2,3,4 \text{ mm}\}$), we manually displaced the NEUROExos joint about 15° in both directions in quasi-static conditions (i.e. $\dot{\theta} \cong 0$). For each value of x_{com} the procedure was iterated ten times in both flexion and extension directions.

The results of this characterization are shown in Fig. 9-a. The measured torque increases linearly with the absolute value of the difference between the equilibrium position and the actual position $\Delta\theta = \theta_{eq} - \theta$. An increase of the common-mode command results in a higher slope of the torque vs. angular displacement curve, and therefore, in an increased passive joint stiffness. The joint stiffness values were estimated through linear fitting (see Fig. 9-a) and are reported in Table II.

Table I Results of the 4-DOF passive mechanism characterization. For each subject, we reported the mean of the absolute value, the maximum and the minimum of γ_f [deg], γ_h [deg] and Δ_h [mm], along with their averaged value overall five subjects.

Subject	#1	#2	#3	#4	#5	Mean ± std
mean($\|\gamma_f\|$)	2.38	2.08	2.05	3.46	2.45	2.49±0.56
max(γ_f)	6.13	6.05	7.08	8.68	8.96	7.38±1.29
min(γ_f)	-9.62	-6.81	-5.97	-14.2	-9.03	-9.12±1.05
mean($\|\gamma_h\|$)	1.90	1.88	1.95	1.73	0.61	1.62±0.56
max(γ_h)	3.22	4.61	5.46	3.05	2.25	3.72±1.29
min(γ_h)	-4.40	-4.13	-4.13	-4.96	-2.16	-3.96±1.05
mean($\|\Delta_h\|$)	0.52	0.84	1.79	1.37	0.86	1.07±0.52
max(Δ_h)	2.89	5.56	9.52	12.5	6.39	7.39±3.73
min(Δ_h)	-2.27	-3.37	-5.12	-5.55	-8.82	-5.03±2.49

Table II Static Characterization: fitting results.

x_{com} [mm]	0	1	2	3	4
K_θ [N·m/rad]	24.6	29.2	36.6	46.4	56.7
RMSE [N·m/rad]	0.06	0.04	0.07	0.06	0.13

Table III Angular step response results.

x_{com} [mm]	0	1	2
Rise Time [s]	0.071	0.067	0.064
Steady-state $\Delta\theta$ [deg]	0.51	0.23	0.12

Table IV Angular chirp response results.

x_{com} [mm]	0	1	2
-3dB bandwidth [Hz]	6.45	6.91	7.24
-3 dB phase [deg]	93.1	89.5	85.8

Table V Mean and the standard deviation of the amplitude difference between the reference and actual angular, and RMSE of $\Delta\theta = \theta_{eq} - \theta$, for the four joint stiffness levels.

x_{com} [mm]	0	1	2	3
Amplitude difference [deg]	22.2±1.4	15.6±2.2	6.1±1.8	2.2±0.4
RMSE of $\Delta\theta$ [deg]	12.1	8.06	5.7	4.96

2) Dynamic characterization

To characterize the dynamic behaviour of the passive-compliance control, we performed a step and chirp response analysis with three different common-mode values. The passive compliance control was also tested in a prototypical robot-in-charge task.

Step response) To characterize the adjustable dynamic behaviour of the variable-compliance joint, the step and chirp response analysis was executed with NEUROExos unloaded, i.e. neither did a subject wear it nor were additionally mock-up masses connected to the moving link. A 30° position step was given at three x_{com} levels: 0, 1 and 2 mm. Twenty repetitions were performed. Fig. 9-b shows the angular trajectory averaged over all the iterations for each stiffness level. As reported in Table III, the rise time decreases proportionally with the increase of the joint stiffness. Moreover, the steady-state angular error $\Delta\theta$ decreases with the level of stiffness (see Table III).

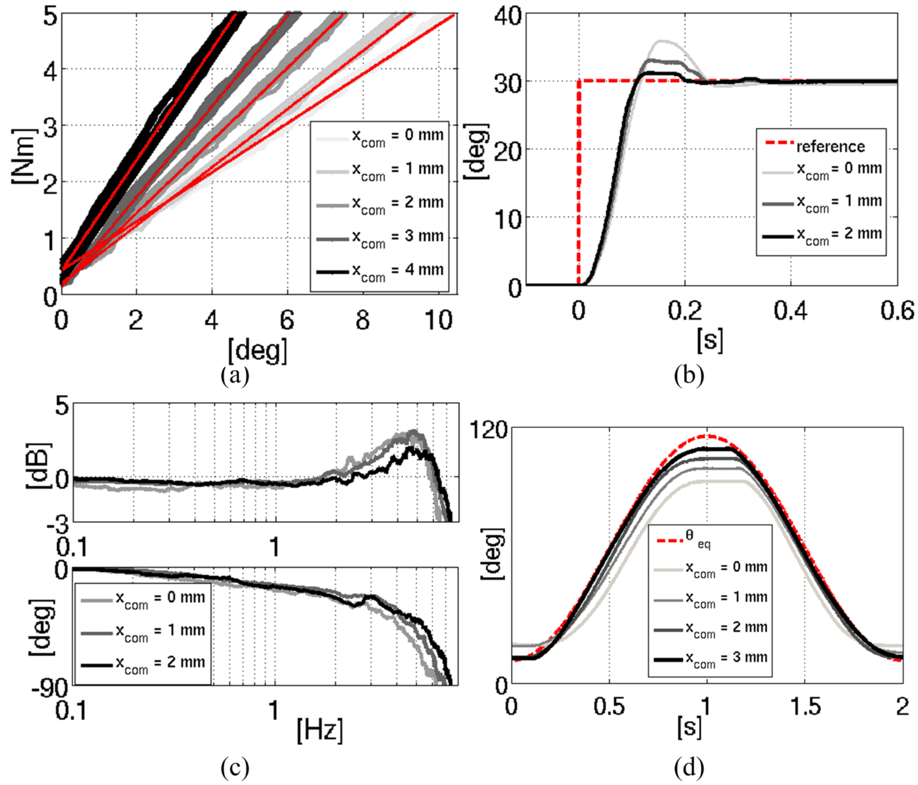

Fig. 9 Experimental characterization of the passive-compliance control: (a) joint torque vs. joint angle displacement curves, (b) step response averaged over 20 iterations, (c) chirp response, (d) sine-wave prototypical task.

The step response is underdamped, with an overshoot of 3.7-19% and a steady-state error of 0.4-1.7% of the amplitude. By increasing the joint stiffness, over-shoot, steady-state error and rise time decrease of 80.8% (from 5.79 to 1.11 deg), 76.4% (from 0.51 to 0.12 deg) and 9.85% (from 0.071 to 0.064 s) respectively, and the peak velocity increases of 11.1%, from 420.1 to 467.2 deg/s.

Steady-state $\Delta\theta$ results from the combined action of the gravity and friction. In fact, the value of $\Delta\theta$ resulting from the sole action of the gravity (which can be computed by means of (13) and assuming m=0.65 kg and L=10.36·10^{-2} m) is lower than the actual one of 0.66°, 0.75° and 0.66°, for x_{com} equal to 1, 2 and 3 mm respectively.

Chirp response) The frequency response of the position control was characterized by displacing the equilibrium position along a linear chirp (frequency 0-8 Hz, duration 480 s, amplitude 30°). The same chirp was repeated for three stiffness levels (x_{com} equal to 0, 1 and 2 mm). The estimated Bode diagram (amplitude and phase) of the system $G(s) = \theta(s)/\theta_{eq}(s)$ was obtained as the ratio between the power spectral density of the measured and input positions. Fig. 9-c shows the resulting Bode plot for each stiffness level and Table IV reports the -3dB bandwidth.

Prototypical robot-in-charge task) In order to evaluate the functionality of the NEUROExos system, a prototypical task was designed and tested on a healthy volunteer (male, 27 years old, 70 Kg). This task simulates a simple rehabilitation procedure, with the subject totally passive and the exoskeleton driving his arm. NEUROExos was programmed to move the equilibrium position along a sinusoidal trajectory (amplitude 105° deg, from 10° to 115°, frequency 0.5 Hz). A two-minute sequence was repeated with four levels of joint stiffness, obtained by setting x_{com} equal to 0, 1, 2, 3 mm. Fig. 9-d shows the commanded and measured angular trajectories for the four levels of stiffness. For the sake of clarity, only one sine wave period is shown. It can be seen that there is an angular difference between the equilibrium and the actual trajectory. By increasing the joint stiffness, the difference $\Delta\theta$ is reduced. Table V reports the mean and standard deviation of the amplitude difference between the equilibrium and the actual angular trajectory, and the RMSE of $\Delta\theta$ over the entire duration of the sine wave, for the four levels of joint stiffness.

C. *Characterization of the torque control*

In order to characterize the closed-loop torque control performance, we analyzed the response of the system to a torque step and a torque chirp command, calculating also the resulting output impedance.

1) *Step and chirp response*

Both step and chirp responses were evaluated in static conditions (i.e. $\dot{\theta} = 0$) with the NEUROExos joint being mechanically blocked and the preloading force set to $F_{com} =$ 10 N.

The step response (from 1 to 7 N·m) was evaluated over 20 iterations. The averaged response is shown in Fig. 10-a. The average value of the rise time was 0.054±0.002 s, the settling time was 0.08±0.003 and the maximum overshoot was 0.27±0.007 N·m.

The chirp response was iterated three times. The reference torque was a chirp signal with mean amplitude of 2 N·m (1 to

3 N·m) and a 0-12 Hz linear frequency sweep over 600 s. The resulting amplitude Bode diagram of the chirp response is reported in Fig. 10-b, and the estimated -3 dB bandwidth was 10.35 Hz.

2) Characterization of the joint output impedance

The output impedance of NEUROExos in torque control mode was tested to assess quantitatively the effort that users need to move the robot in zero torque mode (i.e. $\tau_{des} = 0$).

Impedance was evaluated by moving the joint in zero torque mode and measuring the interaction with force sensors. The transfer function from joint angle to actuator torque is an estimate of the output impedance of NEUROExos in torque control mode [48].

A volunteer wore NEUROExos and performed a quasi-sinusoidal flexion-extension motion, with a torque reference of zero and $F_{com} = 10$ N. The amplitude of the movement was about 30°, the frequency varied linearly in the range 0.3-3.2 Hz for total 40 s of recording. The movement pace was indicated to the user by visual feedback and a metronome. Five iterations were performed for statistical purposes.

Fig. 10-c shows the profile of the interaction torque felt by the subject during the task, along with the profile of the flexion-extension angle. It can been seen that the interaction torque amplitude increases with the motion frequency, reaching 1.80 N·m for 3 Hz motion.

Fig. 10-d shows the Bode plot of the transfer function from the joint angle to the interaction torque. It can be seen that the joint output impedance increases across the spectrum, increasing from about 1 N·m/rad, for a 0.3 Hz motion, up to about 10 N·m/rad at 3.2 Hz.

IV. Discussion

This paper introduced the design of the robotic elbow exoskeleton NEUROExos and presented the results of the experimental activities which aimed at assessing: 1) the NEUROExos pHRI surface, 2) the functionality of the 4-DOF passive mechanism for aligning the robot and user's flexion-extension axes; 3) the performance of the antagonistic actuation, and control system.

A. pHRI surface

The double-shelled structure allowed users with different arm sizes to fit easily in the exoskeleton, thanks to the different sizes of inner shells and to the laxity between inner and outer parts.

Shaped inner shells maximized the human-robot contact area reducing the pressure on the user's skin and improving comfort. This latter aspect was quantitatively assessed in [41], showing typical peak pressures of 7.5 kPa, which is well under the threshold of pain [72], [73]. In addition, despite inner shells encompass the arm, they allowed unconstrained elbow movement thanks to the compliance of the inner layer and of the sylicon belts, which absorbed the volumetric changes of upper-arm and forearm, caused by the muscular activity.

NEUROExos links (outer shells) provided sufficient structural rigidity to transfer torques up to ±15 N·m, despite the low weight (1.65 kg and 0.65 kg for the upper and lower arm, resepctively), thanks to the double-walled carbon-fiber

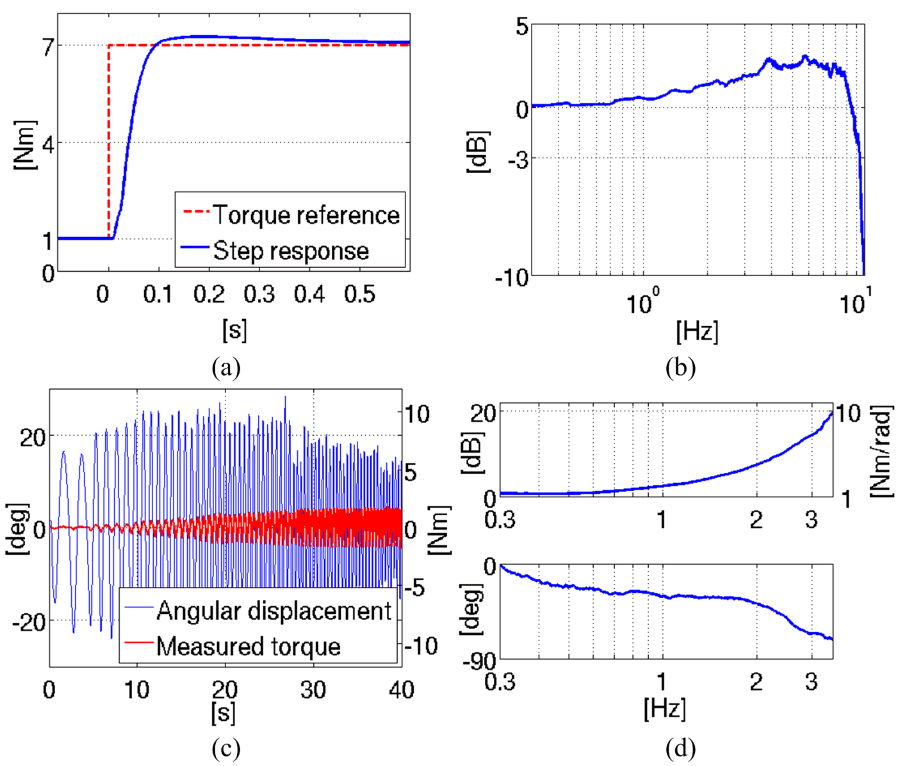

Fig. 10 Experimental characterization of the NEUROExos torque control: (a) step response averaged over 20 iterations, (b) chirp response: amplitude Bode diagram of the transfer function from desired to measured joint torque, (c) characterization of the joint output impedance: angular displacement and interaction torque over a 3 Hz motion range, (d) Bode diagram of the transfer function from angular displacement to interaction torque.

structure.

B. 4-DOF mechanism

The 4-DOF passive mechanism aligns the human and robot rotation axes, and follows the physiological displacement of the elbow axis during flexion-extension movements (see Fig. 3). This mechanism (see Fig. 5), allows a frontal plane rotation $\gamma_f = \pm 15°$ and a horizontal plane rotation $\gamma_h = \pm 21°$. Such ROMs are larger than the displacement of human elbow axis during flexion-extension movements. In fact, human studies showed that the observed frontal plane rotation β_f was ±5° and the horizontal plane rotation β_h was ±3°. Having larger ROM the 4-DOF mechanism can compensate for inter-subject variability [44]-[46], which acts as an offset on the physiological rotation ranges.

Results on five healthy subjects clearly showed that the system can track the elbow axis on the whole movement range. Fig. 8-b shows (for Subject 1) that the rotation angles γ_f and γ_h have a periodic trend along with the task of flexion-extension. Data in Table I, show that the average measured ROM of γ_f and γ_h (respectively equal to 16° and 7°) complies with the ROM of the human elbow axis found in [44]-[46]. Table I also shows that Δ_h has an average measured peak-to-peak ROM of about 10 millimeters. This shows that the rotation axis moves on the horizontal plane during the flexion-extension task and can unload the human joint from undesired translational forces.

C. Passive-compliance and torque control modalities

The experimental characterization of the *passive-compliance control* and the *torque control* proved the usability of NEUROExos in different rehabilitation therapies.

Considering both control modes, the joint stiffness can be tuned from near-zero to about 60 N·m/rad (see Fig. 9 and Fig. 10). The robot is therefore suitable to execute both *robot-in-charge* and *patient-in-charge* exercises and, as a consequence, to assist the movement of users with different level of impairment.

Passive-compliance control) Results of the static characterization (Fig. 9-a and Table I) prove that, by regulating the resting length of the two springs through the x_{com} command, the passive compliance of NEUROExos can be tuned from 24 N·m/rad up to 57 N·m/rad, with x_{com} increasing from 0 to 4 millimeters.

The friction loss given by Bowden cables is relatively low and does not affect significantly the passive elastic behaviour of the joint. This is evidenced by two factors. First, static friction torque (i.e. torque offset in Fig. 9-a) is relatively small: it is 0.5 N·m, equal to 3.5% of the maximum torque output. Second, the sitffness range is close to the nominal values calculated through (6) ($K_\theta \in [22.17 - 54.15]$ N·m/rad), 5-8% lower than the measured. Furthermore, the passive stiffness is highly linear, as shown by the maximum RMSE of the fitting in Fig. 10-a (see Table I), spanning from 0.8% to 2.6% of the maximum torque (i.e. 5 N·m).

The results of the dynamic characterization (Fig. 9-b, c, d and Table II-V) show that the passive-compliance control can be used to displace the user's elbow, along a desired trajectory with different levels of stiffness, full stable dynamic behaviour and adequate bandwidth.

Bode diagram of Fig. 9-c shows that $G(s)$ has a resonance frequency around 4.5-5 Hz. Since most rehabilitation tasks are commonly limited to about 1 Hz [11], [24], [25], [28], the passive-compliance control will guarantee 0 dB and full stability.

Dynamic responses also show that, by increasing the joint stiffness, the system becomes faster (i.e., increase of natural frequency, decrease of rise time) and more damped (i.e., decrease of overshoot and resonance peak). The increased damping is likely due to the Bowden transmission combined with the antagonistic actuation. By increasing the joint stiffness, and thus the preloading force, we get a higher cable friction and, consequenlty, higher joint viscosity and damping [57], [64]. This behaviour enhances the safety of NEUROExos in the stiffer range, with the system capable of better absorbing the effect of undesired (e.g. spastic) movements of the user.

Results of the prototypical task, shown in Fig. 9-d, demonstrate that NEUROExos can drive the human elbow along a desired path in a stable and compliant manner. The *passive-compliance control* softly attracts the human elbow on the desired path and allows a difference between θ and θ_{eq} ($\Delta\theta$), which lowers with K_θ increasing. This feature is important to successful restore the patient's motor function. An adjustable soft assistance allows the adaptation of the torque field to the specific level of impairment of the patient and promotes a gradual active involvement of the subject [11], [74]-[77].

Steady-state $\Delta\theta$ is significantly higher when driving the arm (Fig. 9-d) than when empty (Table III and Table V). This discrepancy is related to the compliant behaviour of the control and actuation system, which allows a $\Delta\theta$ which depends upon the stiffness coefficient and the loading conditions. When the arm is fit in the exoskeleton, gravitational ($m \cong 2$ kg) and inertial ($L \cong 0.35$ m) loads are much higher than in the free movement conditions, and thus $\Delta\theta$ is also higher.

Torque control) By using the same actuation system we could implement a closed-loop torque control. The dynamic characterization of the controller showed a -3dB bandwidth of 10.35 Hz which is sufficiently high for most rehabilitation exercises, given the fact that the human arm can produce muscular torque with a bandwidth of about 3.5 Hz [78].

Importantly, the system shows low output impedance over the typical bandwidth of the human arm movement. This means that if users can actively move their arm, the exoskeleton would have a minimal load on it avoiding to increase the effort. Under the action of the torque control, the joint output impedance is lowered (by 29 dB) to 1 N·m/rad and (by 9 dB) to 10 N·m/rad, during respectively 0.3 Hz and 3.2 Hz motion, compared to the passive impedance of 30 N·m/rad for $F_{com} = 10$ N (see (15)).

Over the band 0.3-3.2 Hz, the measured values of parasitic torque (and stiffness) are relatively low and comparable to the ones reported in state-of-the-art robots [48]. Furthermore, over the typical frequency spectrum of rehabilitation tasks (which is usually upper limited to about 0.5-1 Hz), NEUROExos stiffness is as low as 1.5 N·m/rad, introducing parasitic torque peaks (see also Fig. 10-c, d) which are negligible during the execution of active movements, as demonstrated by the experiments carried out in [38]-[40]. Indeed, as shown in [38], wide bandwidth and minimum parasitic stiffness allow the torque control to be used in a hierarchical control strategy, where a higher control layer sets the desired value of τ_{des} according to a defined assistance strategy which partly compensates for inertia, viscosity and gravity torque of the elbow-NEUROExos coupled system.

Actuation and control hardware modules) The hardware modules of NEUROExos actuation and control system have been designed in order to fit a typical clinical environment for physical rehabilitation. The remote position of the actuation system allows to reduce the encumbrance and mass of the part of the robot that is actually worn by the user. This increase the performance of the systems as well as its acceptability.

V. Conclusion

In this paper, we presented NEUROExos, a novel powered exoskeleton for elbow rehabilitation. NEUROExos possesses three main innovative features: the double-shelled links, the four DOF passive mechanism and a compliant antagonistic actuation system. These features address three important design requirements for a dependable device for physical rehabilitation: (1) a wide and comfortable human-robot physical interface which can gently transmit the interaction torque, (2) the kinematic compatibility between the human and the exoskeleton, to ensure a proper torque transmission to the human joint without the risk of overloading the patient's articulations, and (3) a safe and effective actuation system, which can allow the execution of both *robot-in-charge* and *patient-in-charge* rehabilitation exercises. In this paper, the design and development of the system was described in detail, in associtition with experimental characterization performed to assess its effectiveness in a working scenario.

Future works will aim at using NEUROExos to carry out post-stroke rehabilitation trials inside a clinica setting. Attention will be also devoted to explore design solutions for developing a more compact acutation and control system, based on the use of electromagnetic motors and embedded control units.

References

[1] The world health report 2008, http://www.who.int/whr/2008/en

[2] T. Ingall, "Stroke-Incidence, mortality, morbidity and risk", *Journal of Insurance Medicine*, vol. 36(2), pp. 143-152, 2004.

[3] V. L. Roger et al., "Heart Disease and Stroke Statistics—2011 Update: A Report From the American Heart Association", Circulation 123: e18-209e; published online before print as doi:10.1161/CIR.0b013e3182009701

[4] On the situation of women with disabilities in the European Union, http://www.europarl.europarl.europa.eu/ ,2007.

[5] Healthy ageing: keystone for a sustainable Europe, http://ec.europa.eu/health7ph_information/indicators /docs, 2007.

[6] G. Prange, M. Jannink, C. Groothuis-Oudshoorn, H. Hermens, and M. IJzerman, "Systematic review of the effect of robot-aided therapy on recovery of the hemiparetic arm after stroke", *Journal of Rehabilitation Research and Development*, vol. 43(2), pp. 171-184, 2006.

[7] S. Barreca, S.L. Wolf, S. Fasoli, and R. Bohannon, "Treatment interventions for the paretic upper limb of stroke survivors: a critical review", *Neurorehabilitation and Neural Repair*, vol. 17(4), pp. 220-226, 2003.

[8] H.M. Feys, W.J. De Weerdt, B.E. Selz, G.A. Cox Steck, R. Spichiger, C.E. Vereeck, K.D. Putman, G.A. Van Hoydonock, "Effect of a therapeutic intervention for the hemiplegic upper limb in the acute phase after stroke. A single-blind, randomized, controlled multicenter trial", *Stroke*, vol. 29(4), pp. 785-792, 1999.

[9] G. Kwakkel, R.C. Wagenaar, J.W. Twisk , G.J. Lankhorst, J.C. Koetsier, "Intensity of leg and arm training after primary middle-cerebral-artery stroke: a randomized trial", *Lancet*, vol. 354(9174), pp.191-196, 1999.

[10] G. Kwakkel, B. Kollen, and H. Krebs, "Effects of robot-assisted therapy on upper limb recovery after stroke: A systematic review", *Neurorehabilitation and Neural Repair*, vol. 22, pp.111-121, 2007.

[11] H.I. Krebs, N. Hogan, M.L. Aisen, and B.T. Volpe, "Robot-Aided Neurorehabilitation", *IEEE Transactions on Rehabilitation Engineering* vol. 6(1), pp. 75-87, 1998.

[12] A.C. Lo, P.D. Guarino, L.G. Richards, J.K. Haselkorn, G.F. Wittenberg, D.G. Federman, R.J. Ringer, T.H. Wagner, H.I. Krebs, B.T. Volpe, C.T. Bever, D.M. Bravata, P.W. Duncan, B.H. Corn, A.D.Maffucci, S.E. Nadeau, S.S. Conroy, J.M. Powell, G.D. Huang, and P. Peduzzi, "Robot-Assisted Therapy for Long-Term Upper-Limb Impairment after Stroke", *The New England Journal of Medicine*, vol. 362, pp. 1772-1783, 2010.

[13] S.E. Fasoli, H.I. Krebs, J.Stein, W.R. Frontera, and N. Hogan, "Effects of Robotic Therapy on Motor Impairement and Recovery in Chronic Stroke", *Archives of Physical Medicine and Rehabilitation*, vol. 84(4), pp. 477-482, 2003.

[14] P.S. Lum, C.G. Burgar, D.E. Kenney, and H.F. Machiel Van der Loos, "Quantification of Force Abnormalities During Passive and Active-Assisted Upper-Limb Reaching Movements in Post-Stroke Hemiparesis", *IEEE Transactions on Biomedical Engineering*, vol. 46(6), pp. 652-662, 1999.

[15] S. Micera, M.C. Carrozza, E. Guglielmelli, G. Cappiello, F. Zaccone, C. Freschi, R. Colombo, A. Mazzone, C. Del conte, F. Pisano, G. Minuto, and P. Dario, "A Simple Robotic System for Neurorehabilitation", *Autonomous Robots*, vol. 19(3), pp. 271-284, 2006.

[16] D.J. Reinkensmeyer, C.D. Takahashi, W.K. Timoszyk, A.N. Reinkensmeyer, and L.E. Kahn, "Design of robot assistance for arm movement therapy following stroke", *Advanced Robotics*, vol. 14(7), pp. 625-637, 2001.

[17] R. Loureiro, F. Amirabdollahian, M. Topping, B. Dressen, and W. Harwin, "Upper Limb Robot Mediated Stroke Therapy – GENTLE/s Approach", *Autonomous Robot*, vol.15(1), pp. 35-51, 2003.

[18] D. Mayhew, B. Bachrach, W. Rymer, and R. Beer, "Development of the MACARM-a Novel Cable Robot for upper Limb Neurorehabilitation", in *Proc. of the IEEE International Conference on Rehabilitation Robotics*, Chicago, US, pp. 299-302, 2005.

[19] A. Stienen, E. Hekman, F. Van der Helm, G. Prange, M. Jannink, A. Aalsm, and H. Van der Kooij, "Freebal: Dedicated gravity compensation for the upper extremities", in *Proc. of the International Conference on Rehabilitation Robotics*, Noordwijk, The Netherlands, pp. 804-808, 2007.

[20] Z. Jia-Fan, Y. Can.Jun, C. Ying, Z. Yu, and D. Yi-Ming, "Modeling and control of a curved pneumatic muscle actuator for wearable elbow exoskeleton", *Mechatronics*, vol. 18, pp. 448-457, 2008.

[21] K. Kiguchi, T. Tanaka, and T. Fukuda, "Neuro-fuzzy control of a robotic exoskeleton with EMG signals", *IEEE Transactions on Fuzzy Systems*, vol. 12(4), pp. 481-490, 2004.

[22] J.C. Perry, J. Rosen, and S. Burns, "Upper-Limb Powered Exoskeleton Design", *IEEE/ASME Transactions on Mechatronics*, vol. 12(4), pp. 408-417, 2007.

[23] A. Frisoli, L. Borelli, A. Montagner, S. Marcheschi, C. Procopio, F. Salsedo, M. Bergamasco, M.C. Carboncini, M. Tolaini, and B. Rossi, "Arm rehabilitation with a robotic exoskeleton in Virtual Reality", in *Proc. of IEEE International Conference on Rehabilitation Robotics*, Noordwijk, The Netherlands, pp. 631-642, 2007.

[24] A. Frisoli, F. Salsedo, M. Bergamasco, B. Rossi, and M.C. Carboncini, "A force-feedback exoskeleton for upper-limb rehabilitation in virtual reality", *Applied Bionics and Biomechanics*, 1754-2103, vol. 6(2), pp. 115-126, 2009.

[25] N.G. Tsagarakis and D.G. Caldwell, “Development and Control of a ‘Soft-Actuated’ Exoskeleton for Use in Physiotherapy and Training”, *Autonomous Robots*, vol. 15, pp. 21-23, 2003.

[26] C. Carignan, J. Tang, S. Roderick, and M. Naylor, “A Configuration-Space Approach to Controlling a Rehabilitation Arm Exoskeleton”, in *Proc. IEEE International Conference on Rehabilitation Robotics, (ICORR)*, Noordwijk, The Netherlands, pp. 524-531, 2007.

[27] E. Rocon, J.M. Belda-Lois, A.F. Ruiz, M. Manto, J.C. Moreno, and J.L. Pons, “Design and Validation of a Rehabilitation Robotic Exoskeleton for Tremor Assessment and Suppression”, *IEEE Transactions on Neural Systems and Rehabilitation Engineering*, vol. 15(3), pp. 367-378, 2007.

[28] T. Nef, M. Mihelj, and R. Riener, “ARMin: A robot for patient-cooperative arm therapy”, *Medical and Biological Engineering and Computing*, vol. 45(9), pp. 887-900, 2007.

[29] M. Mihelj, T. Nef, and R. Riener, “ARMin II – 7 DoF rehabilitation: mechanics and kinematics”, in *Proc. of IEEE International Conference on Robotics and Automation (ICRA)*, pp. 4120-4125, 2007.

[30] R.J. Sanchez, E. Wolbrecht, R. Smith, J. Liu, S. Rao, S. Cramer, T. Rahman, J.E. Bobrow, and D.J. Reinkensmeyer, “A Pneumatic Robot for Re-Training Arm Movement after Stroke: Rationale and Mechanical Design”, in *Proc. of the IEEE International Conference on Rehabilitation Robotics (ICORR)*, pp. 500-504, 2005.

[31] R.J. Sanchez, J. Liu, S. Rao, P. Shah, R. Smith, T. Rahman, S.C. Cramer, J.E. Bobrow, and D.J. Reinkensmeyer, “Automating Arm Movement Training Following Severe Stroke: Functional Exercises With Quantitative Feedback in a Gravity-Reduced Environment”, *IEEE Transactions on Neural Systems and Rehabilitation Engineering*, vol. 14(3), pp. 378-389, 2006.

[32] A. Schiele and F.C. van der Helm, “Kinematic Design to Improve Ergonomics in Human Machine Interaction”, *IEEE Transaction on Neural Systems and Rehabilitation Engineering*, vol. 14(4), pp. 456–469, 2006.

[33] A.M. Dollar and H. Herr, “Lower Extremity Exoskeletons and Active Orthoses: Challenges and State-of-the-Art”, *IEEE Transactions on Robotics*, vol. 24, pp. 144-158, 2008.

[34] A.H.A. Stienen, E.E.G. Hekman, F.C.T. van der Helm, and H. van der Kooij, “Self-Aligning Exoskeleton Axes Trough Decoupling of Joint Rotations and Translations, *IEEE Transactions on Robotics*, vol. 25(3), pp. 628-633, 2009.

[35] J.L. Pons, “Rehabilitation Exoskeletal Robotics”, *IEEE Engineering in Medicine and Biology Magazine*, vol. 29(3), pp. 57-63, 2010.

[36] T. Lenzi, S.M.M. De Rossi, N. Vitiello, A. Chiri, S. Roccella, F. Giovacchini, F. Vecchi, and M.C. Carrozza, “The neuro-robotics paradigm: NEURARM, NEUROExos, HANDEXOS”, in *Proc. of the International Conference of the IEEE Engineering in Medicine and Biology Society*, Minneapolis, US, pp. 2430-2433, 2009.

[37] T. Lenzi, N. Vitiello, S.M.M. De Rossi, S. Roccella, F. Vecchi, and M.C. Carrozza, “NEUROExos: a variable impedance powered elbow exoskeleton”, in *Proc. of the IEEE International Conference on Robotics and Automation* (ICRA),Shanghai, China, pp.1419-1426, 2011.

[38] T. Lenzi, S.M.M. De Rossi, N. Vitiello, and M.C. Carrozza, “Proportional EMG control for upper-limb powered exoskeletons”, in *Proc. of the International Conference of the IEEE Engineering in Medicine and Biology Society*, Boston, US, pp. 628-631, 2011.

[39] T. Lenzi, S.M.M. De Rossi, N. Vitiello, and M.C.C. Carrozza, “Intention-Based EMG Control for Powered Exoskeletons”, *IEEE Transactions on Biomedical Engineering*, vol. 59(8), pp. 2180- 2190, 2012.

[40] R. Ronsse, N. Vitiello, T. Lenzi, J. Van den Kieboom, M.C. Carrozza, and A.J. Ijspeert, “Human-robot synchrony: flexible assistance using adaptive oscillators”, *IEEE Transactions on Biomedical Engineering*, vol. 58(4), pp. 1001-1012, 2011.

[41] T. Lenzi, N. Vitiello, S.M.M. De Rossi, A. Persichetti, F. Giovacchini, S. Roccella, F. Vecchi, M.C. Carrozza, "Measuring Human-Robot Interaction on Wearable Robots: a Distributed approach", *Mechatronics*, vol. 21(6), pp. 1123-1131, 2011.

[42] A. Schiele, “Fundamental of Ergonomic Exoskeleton Robots”, Ph.D. dissertation, Technishe Universiteit Delft, 2008.

[43] A. Schiele and F.C.T van der Helm, “Kinematic Design to improve Ergonomics in Human-Machine Interaction”, *IEEE Transactions on Neural Systems and Rehabilitation Engineering*, vol. 14(2), pp. 456-469, 2006.

[44] M. Bottlang, S.M. Madey, C.M. Steyers, J.L. Marsh, and T.D. Brown, “Factors influencing accuracy of screw displacement axis detection with a DC-based electromagnetic tracking system”, *Journal of Biomechanical Engineering*, vol. 120(3), pp. 431-435, 1998.

[45] M. Bottlang, S.M. Madey, C.M. Steyers, J.L. Marsh, and T.D. Brown, “Assessment of elbow joint kinematics in passive motion by electromagnetic motion tracking”, *Journal of Orthopaedic Research*, vol. 18, pp. 195-201, 2000.

[46] T. R. Duck, C.E. Dunning, G.J.W. King, and J.A. Johnson, “Variability and repeatability of the flexion axis at the ulnohumeral joint”, *Journal of Orthopaedic Research*, vol. 21, pp. 399–404, 2003.

[47] A.H.A. Stienen, E.E.G. Hekman, H. ter Braak, A.M.M. Aalsma, F. van der Helm, and H. van der Kooij, “Design of a rotational hydro-elastic actuator for a powered exoskeleton for upper-limb rehabilitation”, *IEEE Transactions on Biomedical Engineering*, vol. 57(3):728-735, 2010.

[48] J.F. Veneman, R. Ekkelenkamp, R. Kruidhof, F.C.T. van der Helm, and H. van der Kooij, “A Series Elastic- and Bowden-Cable-Based Actuation of Use Torque Actuator in Exoskeleton-Type Robots”, *The International Journal of Robotics Research*, vol. 25(3), pp. 261-281, 2006.

[49] M. Zinn, O. Khatib, B. Roth, and J.K. Salisbury, “A New Actuation Approach for Human-Friendly Robot Design”, *The International Journal of Robotics* Research, vol. 23(4-5), pp.379-398, 2004.

[50] G. Pratt and M.M. Williamson, “Series elastic actuators”, in *Proc. of the IEEE International Conference on Intelligent Robots and Systems*, Pittsburgh, US, pp. 339-406.

[51] J. Oblak, I. Cikajlo, and Z. Matjačić, “Universal Haptic Drive: A Robot for Arm and Wrist Rehabilitation”, *IEEE Transactions on Neural Systems and Rehabilitation Engineering*, vol. 18(3), pp. 293-302, 2010.

[52] R. Schiavi, G. Grioli, S. Sen, and A. Bicchi, “VSA-II: a novel prototype of variable stiffness actuator for safe and performing robots interacting with humans”, in *Proc. of the IEEE International Conference on Robotics and Automation*, pp. 2171-2176, 2008.

[53] S.A. Migliore, E.A. Brown, and S.P. De Weerth, “Biologically inspired joint stiffness control”, in *Proc. of the IEEE International Conference on Robotics and Automation*, pp. 4508-4513, 2005.

[54] K. Koganezawa, T. Inaba, and T. Nakazawa, “Stiffness and angle control of antagonistically driven joint”, in *Proc. of the IEEE International Conference on Biomedical Robotics and Biomechatronics*, pp. 1007-1013, 2006.

[55] D.G. Caldwell, G.A. Medrano-Cerda, and M. Goodwin, “Control of pneumatic muscles actuators”, *IEEE Control System Magazine*, vol. 15(1), pp. 40-48, 1995.

[56] N. Vitiello, T. Lenzi, S.M.M. De Rossi, S. Roccella, M.C. Carrozza, “A sensorless torque control for Antagonistic Driven Compliant Joints”, *Mechatronics*, vol. 20(3), pp. 355-367, 2010.

[57] T. Lenzi, N. Vitiello, J. McIntyre, S. Roccella, M.C. Carrozza, “A robotic model to investigate the human motor control”, *Biological Cybernetics*, vol. 105(1), pp. 1-19, 2011.

[58] E. Cattin, S. Roccella, N. Vitiello, I. Sardellitti, K.A. Panagiotis, P. Vacalebri, F. Vecchi, M.C. Carrozza, K. Kyriakopulos, and P. Dario, “Design and Development of a Novel Robotic Platform for Neuro-Robotics Applications: the NEURobotics ARM (NEURARM)”, *Advanced Robotics*, Special Issue on Robotics platforms for Neuroscience, vol. 22, pp. 3-37, 2008.

[59] N. Vitiello, E. Cattin, S. Roccella, F. Giovacchini, F. Vecchi, M.C. Carrozza, and P. Dario, “The NEURARM towards a Platform for Joint Neuroscience Experiments on Human Motion Control Theories”, in *Proc. IEEE International Conference on Intelligent Robots and Systems*, San Diego, pp. 1852-1857, 2007.

[60] N. Vitiello, T. Lenzi, J. McIntyre, S. Roccella, E. Cattin, F. Vecchi, and M.C. Carrozza, “Characterization of the NEURARM bio-inspired joint position and stiffness open loop controller”, in *Proc. of IEEE International Conference on Biomedical Robotics and Biomechatronics*, Scottsdale, US, pp. 138-143, 2008.

[61] M.O. Abe and N. Yamada, “Modulation of elbow joint stiffness in a vertical plane during cyclic movement at lower or higher frequencies than natural frequency”, *Experimental Brain Research*, vol. 153, pp. 394-299, 2003.

[62] D.W. Franklin, E. Burdet, R. Osu, M. Kawato, and T.E. Milner, “Functional significance of stiffness in adaptation of multijoint arm movements to stable and unstable dynamics, *Experimental Brain Research*, vol. 151, pp. 145-157, 2003.

[63] A. Schiele, P. Letier, R. van der Linde, and F.C.T. van der Helm, “Bowden cable actuator for force-feedback exoskeletons”, in *Proc. of IEEE International Conference on Intelligent Robots and Systems*, pp. 3599-3604, 2006.

[64] A. Chiri, N. Vitiello, F. Giovacchini, S. Roccella, F. Vecchi, and M.C. Carrozza, "Mechatronic Design and Characterization of the Index Finger Module of a Hand Exoskeleton for Post-stroke Rehabilitation", *IEEE/ASME Transactions on Mechatronics*, in press, doi: 10.1109/TMECH.2011.2144614, 2011.

[65] N. Hogan, "An organizing principle for a class of voluntary movements", *Journal of Neuroscience*, vol. 4, pp. 2745-2754, 1984.

[66] N. Hogan, E. Bizzi, and F.A. Mussa-Ivaldi, T. Flash, "Controlling multijoint motor behaviour", *Exercise and Sport Sciences Reviews*, vol. 15, pp. 153-190, 1987.

[67] E. Bizzi, N. Accornero, W. Chapple, and N. Hogan, "Posture control and trajectory formation during arm movement", *Journal of Neuroscience*, vol. 4, pp. 2738-2744, 1984.

[68] A. Polit and E. Bizzi, "Characteristics of motor programs underlying arm movements in monkeys", *Journal of Neurophysiology*, vol. 42, pp. 183-194, 1979.

[69] A.G. Feldman, "Functional tuning of the nervous system with control of movement or maintenance of steady posture, II: controllable parameters of the muscles", *Biophysics*, vol. 11, pp. 565-578, 1966.

[70] A. Bicchi and G. Tonietti, "Fast and Soft Arm Tactics: Dealing with the Safety-Performance Trade-Off in Robot Arms Design and Control", *IEEE Robotics and Automation Magazine*, vol. 11(2), pp. 22-33, 2004.

[71] I.A. Kapandji, "Fisiologia articolare. Arto Superiore", Editions MALOINE, Paris, France, 2002.

[72] J.L. Pons, "Wearable Robots: Biomechatronic Exoskeletons", Wiley-Blackwell, Hoboken (2008).

[73] S.M.M. De Rossi, N. Vitiello, T. Lenzi, R. Ronsse, B. Koopman, A. Persichetti, F. Vecchi, A.J. Ijspeert, H. van der Kooij, and M.C. Carrozza, "Sensing Pressure Distribution on a Lower-Limb Exoskeleton Physical Human-Machine Interface", *Sensors*, vol. 11(1), pp.: 207-227, 2011.

[74] M. Ziegler, H. Zhong, R.R. Roy, and V. Reggie Edgerton, "Why Variability Facilitates Spinal Learning", *Journal of Neuroscience*, vol. 30(32), pp. 10720-10726, 2010.

[75] L.L. Cai, A.J. Fong, C.K. Otoshi, Y. Liang, J.W. Burdick, R.R. Roy, and V. Reggie Edgerton, "Implications of Assist-As-Needed Robotic Step Training after a Complete Spinal Cord Injury on Intrinsic Strategies of Motor Learning", *Journal of Neuroscience*, vol. 26(41), pp. 10564-10568, 2006.

[76] J.L. Patton, M.E. Stoykov, M. Kovic, and F.A. Mussa-Ivaldi, "Evaluation of robotic training forces that either enhance or reduce error in chronic hemiparetic stroke survivors", *Experimental Brain Research*, vol. 168, pp. 368-383, 2006.

[77] H.I. Krebs, J.J. Palazzolo, L. Dipietro, M. Ferraro, J. Krol, K. Rannekleiv, B.T. Volpe and N. Hogan, "Rehabilitation Robotics: Performance-Based Progressive Robot-Assisted Therapy Autonomous Robots", *Autonomous Robot*, vol. 15(1), pp. 7-20, 2003.

[78] H.S. Milner-Brown, R.B. Stein, and R. Yemm, "The contractile properties of human motor units during voluntary isometric contractions", *Journal of Physiology*, vol. 228, pp.: 285-306, 1973.

Nicola Vitiello (M'12) is Assistant Professor at The BioRobotics Institute of Scuola Superiore Sant'Anna. He received the M.Sc. degree in Biomedical Engineering (cum laude) both from the University of Pisa, Italy, in 2006, and from Scuola Superiore Sant'Anna, Italy, in 2007. He received the Ph.D. degree in Biorobotics from the Scuola Superiore Sant'Anna, Italy, in 2010. His main research interests include the development of wearable robotic devices for human motion assistance and rehabilitation and of robotic platforms for neuroscientific investigations. He is author and co-author of 11 ISI papers and 23 peer-review conference-proceedings papers. He served as scientific secretary of the EU FP7 CA-RoboCom project, and he is currently project manager of the EU FP7 CYBERLEGs Project.

Tommaso Lenzi (S'10) received the B.Sc and M.Sc in Biomedical Engineering (cum laude) from University of Pisa in 2005 and 2008 respectively. Since 2008 is a PhD student in BioRobotics at The BioRobotics Institute (former ARTS Lab) of Scuola Superiore Sant'Anna (Italy). From August 2011 to February 2012 he has been a Visiting Research Scientist at the Mechanical Engineering Department of University of Delaware (USA) under the supervision of Dr. S. K. Agrawal. His main research interests lies in between robotics, biomechanics and neurophysiology with a major in design and control of powered exoskeletons for human assistance and rehabilitation. He is author and co-author of 8 ISI Journal papers and 16 peer-review conference-proceedings papers and serves as a reviewer of IEEE/ASME Transaction on Mechatronics, and Applied Bionics and Biomechanics. From 2010 Mr. Lenzi is student member of IEEE, RAS and EMBS scientific society.

Stefano Roccella received his Laurea Degree in Aeronautical Engineering from the University of Pisa. In 1999 he joined The BioRobotics Institute of Scuola Superiore Sant'Anna as a Research Assistant. In March 2006, he received his Ph.D. in Robotics at University of Genova. Currently, he is a PhD Technical Research Manager at Scuola Superiore Sant'Anna. His research interests are in the fields of mechatronic systems, humanoid robotics, biomedical robotics, rehabilitation engineering, biomechatronics, and MEMS design and development.

Stefano Marco Maria De Rossi (S'10) received the M.Sc. degree in control engineering (cum laude) both from the University of Pisa, Italy and from Scuola Superiore Sant'Anna, Pisa, Italy in 2009. He is currently working toward the Ph.D. degree in Biorobotics at The BioRobotics Institute, Scuola Superiore Sant'Anna, Pisa, Italy. His current research interests include wearable robotics, human-robot interfaces and robotics for upper and lower limb rehabilitation.

Emanuele Cattin received his Laurea Degree in Mechanical Engineerig from the University of Padova in July 2003, and the Ph.D. degree in Robotics from the University of Genova in 2008. In January 2004 he joined the Advanced Robotic Technology and Systems (ARTS) Lab (now The BioRobotics Institute) at the Scuola Superiore Sant'Anna in Pisa, Italy., where he conducted research activities in the field of wearable robotics until 2009.

Francesco Giovacchini received his M.S. degree in Mechanical Engineering in 2006. Since January 2007 he has worked at The BioRobotics Institute of Scuola Superiore Sant'Anna. His research interests are in the field of biomechatronics, and more specifically in the development of robotic platforms and wearable devices for rehabilitation and neurobotics.

Fabrizio Vecchi (M'04) received the University Degree (Laurea) in electrical engineering from the University of Pisa, Italy, in 1999 and the Ph.D. in Robotics from the University of Genova in 2003. He is Post-Doc research scientist at The BioRobotics Institute of Scuola Superiore Sant'Anna. During his career he participated in the design and development of human-machine interfaces, biomechatronic prosthetic and robotic hands, passive and active orthoses, flexible sensory skin, and technical assistive devices. He is co-inventor of 7 national and international patents, and is co-author of more than 40 scientific papers published on ISI journals and on proceedings of international conferences.

Maria Chiara Carrozza (Master in Physics at University of Pisa in 1990, PhD in Engineering at Scuola Superiore Sant'Anna in 1994) is Full Professor of Biomedical Engineering and Robotics at Scuola Superiore Sant'Anna (SSSA). Since Nov. 2007, she is Rector of Scuola Superiore Sant'Anna. Her research interests are in ambient assisted living, biorobotics, rehabilitation engineering, bionics, cybernetic hands, humanoid robotics, systems for functional replacements and augmentation, biomechatronic interfaces, tactile sensors and artificial skin. She coordinates several research projects funded by national and European grants in the area of rehabilitation engineering, prosthetics, human-machine interfaces and exoskeleton for functional replacement and assistance. She is author of several scientific papers (more than 60 ISI papers and more than 100 papers in referred conference proceedings) and of 12 national and international patents. She is Member of IEEE Robotics and Automation and Engineering in Medicine and Biology Societies.